Impact of the symmetry energy on the outer crust of nonaccreting neutron stars

X. Roca-Maza[1] and J. Piekarewicz[2]
[1]*Departament d'Estructura i Constituents de la Matèria, Facultat de Física, Universitat de Barcelona, Diagonal 647, E-08028 Barcelona, Spain*
[2]*Department of Physics, Florida State University, Tallahassee, Florida 32306, USA*
(Received 16 May 2008; published 21 August 2008)

The composition and equation of state of the outer crust of nonaccreting neutron stars is computed by using accurate nuclear mass tables. The main goal of the present study is to understand the impact of the symmetry energy on the structure of the outer crust. First, a simple "toy model" is developed to illustrate the competition between the electronic density and the symmetry energy. Then, realistic mass tables are used to show that models with a stiff symmetry energy—those that generate large neutron skins for heavy nuclei—predict a sequence of nuclei in the stellar environment that is more neutron rich than their softer counterparts. This result may be phrased in the form of a correlation: The larger the neutron skin of ^{208}Pb, the more exotic the composition of the outer crust.

DOI: 10.1103/PhysRevC.78.025807 PACS number(s): 26.60.Kp, 26.60.Gj, 21.65.Ef, 21.10.Dr

I. INTRODUCTION

Neutron stars are gold mines for the study of nuclear systems under extreme conditions of density and isospin asymmetry [1,2]. Spanning many orders of magnitude in density, neutron stars display exotic phases that cannot be realized under normal laboratory conditions. Whereas the most common perception of a neutron star is that of a uniform mantle of neutrons packed to densities that may exceed that of normal nuclei by up to an order of magnitude, the reality is far different and much more interesting. First, although the uniform liquid mantle (also known as the outer core) is indeed composed mostly of neutrons, a small fraction of protons and an equal number of charged leptons (i.e., electrons and perhaps even muons) must be present to maintain beta equilibrium. The precise proton fraction in the neutron star is controlled by the *symmetry energy*, a quantity that imposes a penalty on the system as it departs from the isospin symmetric limit of equal number of neutrons and protons. Second, at densities that are below nuclear matter saturation density the uniform phase becomes unstable against density fluctuations. This nonuniform region of the neutron star constitutes the *crust*, which itself is divided into an inner and an outer region (see Fig. 1). In the outer crust—the main focus of the present study—the system is organized into a Coulomb lattice of neutron-rich nuclei embedded in a uniform electron gas [3]. As the density increases, nuclei become progressively more neutron rich until the neutron drip region is reached; this region defines the boundary between the outer and the inner crust. As in the case of the outer crust, the inner crust also consists of a Coulomb lattice of neutron-rich nuclei embedded in a uniform electron gas. Now, however, a uniform neutron vapor permeates the system. As the density continues to increase in the inner crust, the system is speculated to morph into a variety of complex and exotic structures, such as spheres, cylinders, rods, and plates—collectively known as *nuclear pasta* [4–6]. As the density increases even further, uniformity is eventually restored at about one-third of normal nuclear matter saturation density. Finally, at ultra high densities it has been established that the ground state of hadronic matter becomes a color superconductor in a color-flavor-locked (CFL) phase [7,8]. It is unknown, however, whether the density at the core of a neutron star may reach the extreme values required for the CFL phase to develop. Thus, other exotic phases—such as meson condensates, hyperonic matter, and/or quark matter—may be more likely to harbor the core of neutron stars. Figure 1 is believed to represent a plausible rendition of the structure of a neutron star.

As stated earlier, the main focus of our present study is the outer crust of the neutron star. In particular, we are interested in studying the sensitivity of the composition of the outer crust to the model dependence of the symmetry energy. The outer crust comprises a region spanning about seven orders of magnitude in density: from about 10^4 g/cm^3 to a neutron drip density of about 4×10^{11} g/cm^3 [3]. Although these densities are small relative to nuclear matter saturation density (2.5×10^{14} g/cm^3), the electrons (present to maintain charge neutrality) at such densities are no longer bound to nuclei and move freely throughout the crust. Moreover, at these low nuclear densities it is energetically favorable for the nuclei to arrange themselves in a crystalline lattice. At the lowest densities, the electronic contribution is negligible, so the Coulomb lattice is populated by ^{56}Fe nuclei. However, as the density increases and the electronic contribution becomes important, ^{56}Fe ceases to be the most energetically favorable nucleus. Instead, it becomes energetically advantageous for the system to lower its electron fraction by having the energetic electrons capture onto protons, with the excess energy carried away by neutrinos. The resulting nuclear lattice is now formed by nuclei having a slightly lower proton fraction than ^{56}Fe (e.g.,^{62}Ni). As the density continues to increase, the nuclear system evolves into a Coulomb lattice of progressively more neutron rich nuclei until the critical neutron drip density is reached. The essential physics of the outer crust is then nicely captured by a "tug-of-war" between an electronic contribution and the nuclear symmetry energy, with the former favoring neutron-rich nuclei and the latter favoring fairly symmetric

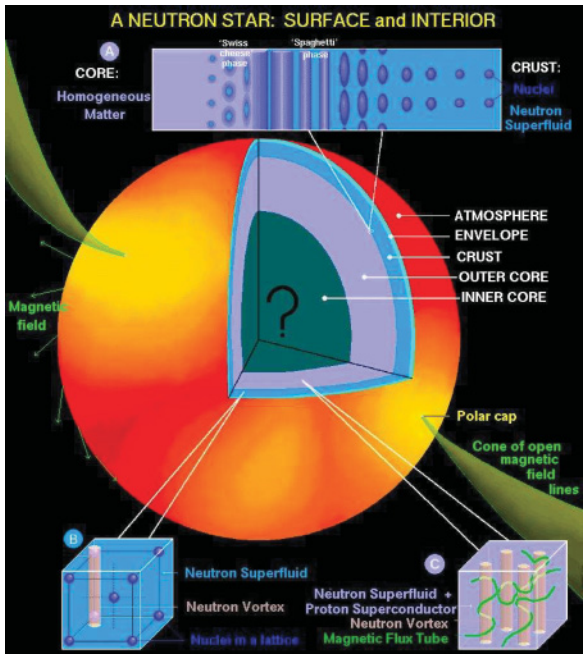

FIG. 1. (Color online) Rendition of the assumed structure and phases of a neutron star. (Figure courtesy of Dany Page.)

ones. The neutron-rich nuclei that populate the Coulomb lattice in the outer crust are on average more dilute than their more symmetric counterparts because of the development of a neutron skin. As a result, these nuclei may become sensitive to the symmetry energy below nuclear matter saturation density. However, whereas the symmetry energy is relatively well known around saturation density, its density dependence (e.g., its slope) is poorly constrained. This may affect the composition of the crust.

Although some theoretical constraints are starting to emerge [9,10], the density dependence of the symmetry energy remains largely unknown. Indicative of this fact is that accurately calibrated models of nuclear structure (both relativistic and nonrelativistic) that reproduce a variety of ground-state properties across the periodic table differ significantly in their predictions for the density dependence of the symmetry energy. Yet these same models have been used to uncover a strong correlation between the pressure of pure neutron matter at saturation density and the neutron skin of heavy nuclei: the larger the pressure the larger the neutron skin [11,12]. (Note that the pressure of pure neutron matter equals that of the symmetry energy at saturation density.) This fact may be illustrated by using the two accurately calibrated models that will be employed throughout this manuscript, namely, NL3 [13,14] and FSUGold [15]. Whereas NL3 predicts a pressure at saturation density of $P_0 \approx 6\,\mathrm{MeV/fm^3}$ and a corresponding neutron skin in ^{208}Pb of $R_n - R_p \approx 0.28$ fm, FSUGold predicts the significantly lower values of $P_0 \approx 3\,\mathrm{MeV/fm^3}$ and $R_n - R_p \approx 0.21$ fm, respectively. The upcoming Parity Radius Experiment (PREx) at the Jefferson Laboratory will provide a unique experimental constraint on the density dependence of the symmetry by measuring the skin thickness of ^{208}Pb accurately and model independently via parity-violating electron scattering [16,17]. The correlation between the density dependence of the symmetry energy and the neutron skin of heavy nuclei opened new horizons in nuclear astrophysics. Novel correlations between the neutron skin of ^{208}Pb and a myriad of neutron-star observables were developed as a result of the similar composition of the neutron skin of a heavy nucleus and the inner crust/outer core of a neutron star [18–23]. One particularly interesting correlation of direct relevance to the crustal region is a "data-to-data" relation between the neutron skin of ^{208}Pb and the crust-to-core transition density [18].

The recent observations of intense pulses of energetic γ rays followed by fainter periodic signals emitted from highly magnetized neutron stars (or "magnetars") are sure to provide an additional new tool in the study of neutron-star structure [24–27]. The discovery of high-frequency oscillations in the tails of giant flares from soft gamma repeaters (i.e., magnetars with magnetic fields in excess of 10^{14} gauss [28–30]) are believed to be associated with seismic vibrations of the neutron star crust. Early theoretical models that assume a liquid-core/solid-crust interface suggest torsional shear oscillations of the crust as the most likely modes of excitation in a magnetar. The shear modulus of the crust acts as a restoring force for these modes and such a structural property is highly sensitive to the composition of the crust and, thereby, to the nuclear matter equation of state. Indeed, the shear-mode oscillations depend strongly on the neutron star mass, radius, and *crustal composition*—all properties sensitive to the equation of state [24]. Moreover, *ratios* of frequencies with different nodal structures may be used to determine the thickness of the crust, an observable highly sensitive to the equation of state and particularly to the density dependence of the symmetry energy [25,26]. Hence, as techniques continue to improve, we expect that neutron-star seismology will provide stringent limits on the equation of state of neutron-rich matter.

The manuscript has been organized as follows. The formalism required to compute the composition and equation of state of the outer crust is developed in Sec. II. In Sec. III we employ several realistic nuclear-mass models to compute the structure of the outer crust. Although not nearly as comprehensive as the recent study performed by Rüster, Hempel, and Schaffner-Bielich [31], ours includes a simple "toy model" that provides critical insights into the role played by the symmetry energy. Moreover, in the same section we illustrate the impact of the density dependence of the symmetry energy on the sequence of neutron-rich nuclei present in the outer crust. Our results and conclusions are summarized in Sec. IV.

II. FORMALISM

In this section we develop the formalism necessary to understand the composition and equation of state of the outer crust of a neutron star. The formalism follows closely the seminal ideas introduced by Baym, Pethick, and Sutherland back in 1971 [3]. For more recent references that employ modern nuclear mass tables see Refs. [31–33]. The central question that one aims to answer is the following: What is the ground state of cold, fully catalyzed matter for densities

between complete ionization ($\rho \approx 10^4$ g/cm^3) and "neutron drip" ($\rho \approx 10^{11}$ g/cm^3)? Since at these densities uniform matter is unstable against cluster formation, a Coulomb lattice of nuclei embedded in a uniform free Fermi gas of electrons is formed. Thus, the composition of the outer crust is determined by that nucleus (with neutron number N, proton number Z, and baryon number $A = N + Z$) that minimizes—for each density—the total energy per nucleon of the system. In the outer crust (i.e., before neutron drip) the *energy per nucleon* consists of three different contributions: nuclear, electronic, and lattice. That is,

$$\varepsilon(A, Z; n) = \varepsilon_n + \varepsilon_e + \varepsilon_\ell, \tag{1}$$

where the baryon density is denoted by $n \equiv A_{\rm total}/V$. The nuclear contribution to the total energy per nucleon is simple and independent of the density. It is given by

$$\varepsilon_n(N, Z) \equiv \frac{M(N, Z)}{A},$$

with

$$M(N, Z) = Nm_n + Zm_p - B(N, Z). \tag{2}$$

Here $M(N, Z)$ is the nuclear mass, $B(N, Z)$ is the corresponding binding energy, and m_n and m_p are neutron and proton masses, respectively.

The electronic contribution—at least at the densities of interest ($\rho \gtrsim 10^4$ g/cm^3)—is modeled as a degenerate free Fermi gas [3]. That is,

$$\varepsilon_e(A, Z; n) = \frac{\mathscr{E}_e}{n} = \frac{1}{n\pi^2}\int_0^{p_{\rm Fe}} p^2\sqrt{p^2 + m_e^2}\, dp, \tag{3}$$

where $\mathscr{E}_e$, m_e, and $p_{\rm Fe}$ are the electronic energy density, mass, and Fermi momentum, respectively. Note that the electronic Fermi momentum and baryon density are related as follows:

$$p_{\rm Fe} = (3\pi^2 n_e)^{1/3} = (3\pi^2 yn)^{1/3} \equiv y^{1/3} p_F, \tag{4}$$

where the electron fraction $y \equiv Z/A$ has been defined. Moreover, for future convenience the following definition of the overall Fermi momentum has been introduced:

$$p_F = (3\pi^2 n)^{1/3}. \tag{5}$$

As the integral in Eq. (3) may be evaluated analytically, the electronic contribution may be computed in closed form. That is,

$$\varepsilon_e(A, Z; n) = \frac{m_e^4}{8\pi^2 n}\left[x_F y_F\left(x_F^2 + y_F^2\right) - \ln(x_F + y_F)\right], \tag{6}$$

where dimensionless Fermi momentum and energy have been defined as follows:

$$x_F \equiv \frac{p_{\rm Fe}}{m_e} \quad \text{and} \quad y_F \equiv \frac{\epsilon_{\rm Fe}}{m_e} = \sqrt{1 + x_F^2}. \tag{7}$$

We now discuss the last term in Eq. (1). Whereas the Coulomb repulsion within the individual nuclei has been properly included in Eq. (2), the Coulomb repulsion among nuclei as well as their interactions with the uniform electron background has not. At the densities and temperatures of relevance to the outer crust, namely, large enough for full ionization but small enough for the Coulomb repulsion among nuclei to dominate over their kinetic energy, Wigner has shown (in the context of the electron gas) that the system will crystallize into a body-centered-cubic lattice [34–36]. The last term in Eq. (1) represents the lattice contribution to the energy per particle. The calculation of the potential energy of the Coulomb lattice is complicated. It consists of divergent contributions that must be canceled as required by the overall charge neutrality of the system. Fortunately, accurate numerical calculations for the electron gas have been available for a long time [37,38] and these results can be readily generalized to the present case [3]. Indeed, the lattice energy per nucleus may be written as

$$\frac{E_\ell}{N_c} = -(1.81962)\frac{(Ze)^2}{a} = -(1.79186)\frac{(Ze)^2}{2r_0}, \tag{8}$$

where N_c is the number of nuclei (i.e., A-body clusters), a is the lattice constant, and r_0 is a length scale related to the volume per nuclei. For the particular case of a body-centered-cubic lattice, these quantities are related in the following way:

$$n_c a^3 = \frac{N_c}{V}a^3 = 2 \quad \text{or} \quad \left(\frac{a}{2r_0}\right) = \left(\frac{\pi}{3}\right)^{1/3}. \tag{9}$$

Using the fact that the number of nuclei is related to the total baryon number of the system as

$$N_c = \frac{A_{\rm total}}{A} = \frac{N_{\rm total}}{N} = \frac{Z_{\rm total}}{Z}, \tag{10}$$

we can write the lattice contribution to the energy per baryon in closed form as follows:

$$\varepsilon_\ell(A, Z; n) = -\frac{(1.79186)}{A^{4/3}}\frac{(Ze)^2}{2R_0}. \tag{11}$$

Note that here R_0 refers to the length scale associated with the volume per *baryon* ($r_0 = A^{1/3}R_0$). That is,

$$R_0 = \left(\frac{3}{4\pi n}\right)^{1/3} = \left(\frac{9\pi}{4}\right)^{1/3} {p_F}^{-1}. \tag{12}$$

By using these definitions, the lattice contribution becomes equal to

$$\varepsilon_\ell(A, Z; n) = -C_\ell \frac{Z^2}{A^{4/3}} p_F \quad (\text{with } C_\ell = 3.40665 \times 10^{-3}). \tag{13}$$

For completeness, the full expression for the energy per baryon is now displayed in terms of the individual *nuclear, electronic,* plus *lattice* contributions:

$$\begin{aligned}\varepsilon(A, Z; n) &= \frac{M(N, Z)}{A} + \frac{m_e^4}{8\pi^2 n}\left[x_F y_F\left(x_F^2 + y_F^2\right) - \ln(x_F + y_F)\right] \\ &\quad - C_\ell \frac{Z^2}{A^{4/3}} p_F.\end{aligned} \tag{14}$$

Note that given A, Z, and $n = A_{\rm total}/V$, the only unknown quantity in this expression is the nuclear mass $M(N, Z)$. Although experimentally available for a large number of nuclei around the line of stability, nuclear masses near the drip line are unknown, thereby making the need for theoretical extrapolations unavoidable. As crustal properties become

better determined, nuclear masses at the drip line will be strongly constrained. Alternatively, the advent of facilities capable of producing beams of rare isotopes to explore the limits of nuclear existence will place strong constraints on crustal properties.

Having computed the energy per baryon of the system, we are now in a position to compute two additional thermodynamic properties that are essential for the understanding of both the structure and composition of the outer crust. These are the equation of state, namely, the relation between pressure and density, and the chemical potential. Recall that in modeling the outer crust the central assumption is that of thermal, hydrostatic, and chemical equilibrium. Thus, complete equilibrium demands the equality of temperature, pressure, and chemical potential at each layer of the outer crust.

At zero temperature and for a constant number of particles, the pressure of the system may be computed from the total energy of the system. As the individual nuclei do not contribute to the pressure, one must only compute the electronic and lattice contributions. In particular, the electronic contribution at zero temperature is given by

$$P_e \underset{T=0}{=} -\left(\frac{\partial E_e}{\partial V}\right)_Z = \frac{x_F}{3}\left(\frac{\partial \mathscr{E}_e}{\partial x_F}\right) - \mathscr{E}_e = \frac{m_e^4}{3\pi^2}\left(x_F^3 y_F - \frac{3}{8}\left[x_F y_F\left(x_F^2 + y_F^2\right) - \ln(x_F + y_F)\right]\right). \tag{15}$$

Similarly, the lattice contribution to the pressure is given by the following simple expression:

$$P_\ell \underset{T=0}{=} -\left(\frac{\partial E_\ell}{\partial V}\right)_{A,Z} = -\frac{n}{3} C_\ell \frac{Z^2}{A^{4/3}} p_F. \tag{16}$$

In this manner the full (*electronic* plus *lattice*) contribution to the pressure may be written as

$$P(A, Z; n) = \frac{m_e^4}{3\pi^2}\left(x_F^3 y_F - \frac{3}{8}\left[x_F y_F\left(x_F^2 + y_F^2\right) - \ln(x_F + y_F)\right]\right) - \frac{n}{3} C_\ell \frac{Z^2}{A^{4/3}} p_F. \tag{17}$$

As alluded to earlier, full equilibrium in the system is established by demanding that the temperature, pressure, and chemical potential—but not necessarily the baryon density—be continuous throughout the outer crust. As the temperature of the system is assumed to be equal to zero, the only remaining thermodynamic observable to calculate is the chemical potential. At zero temperature, the Gibbs free energy and the total energy of the system are related by a Legendre transform ($G = E + PV$). That is,

$$\mu(A, Z; P) = \frac{G(A, Z; P)}{A_{\text{total}}} = \varepsilon(A, Z; n) + \frac{P}{n} = \frac{M(N, Z)}{A} + \frac{Z}{A}\mu_e - \frac{4}{3} C_\ell \frac{Z^2}{A^{4/3}} p_F, \tag{18}$$

where $\mu_e = \sqrt{p_{\text{Fe}}^2 + m_e^2}$ is the electronic chemical potential. Note that the chemical potential is a function of the pressure whereas the energy per baryon is a function of the baryon density. The transformation from one into the other is accomplished through Eq. (17). Also note that as hydrostatic and chemical equilibrium must be maintained throughout the star, it is convenient to compute the composition of the outer crust by minimizing the Gibbs free energy per particle (i.e., μ) at constant pressure rather than by minimizing the energy per particle at constant baryon density. This procedure will be carried out in the next section.

III. RESULTS

In this section results will be presented for the structure and composition of the outer crust. The implementation of the ideas developed in the previous section will be carried out by using various models for nuclear masses. Two of these models are based on sophisticated microscopic/macroscopic models that yield root-mean-square (rms) errors of only a fraction of an MeV when compared to large databases of available experimental nuclear masses [39,40]. These two models are the ones by Duflo and Zuker [41–43] and the finite range droplet model of Möller, Nix, and collaborators [44,45]. The other two models are based on accurately calibrated microscopic approaches that employ a handful of empirical parameters to reproduce the ground-state properties of finite nuclei and some collective excitations [13–15]. Although these microscopic approaches are successful, their rms errors are significantly larger than those obtained with the microscopic/macroscopic models. Yet one of the great advantages of the microscopic models is the ability to systematically study the impact of unknown physics on crustal properties. First and foremost, we are interested in understanding how models that are equally successful in describing available ground-state properties of finite nuclei differ in their predictions of exotic (neutron-rich) nuclei.

A. Toy model of the outer crust

Although the structure and composition of the crust will be ultimately computed using sophisticated mass formulas, we start by introducing a "toy model" that despite its simplicity captures the essential physics of the outer crust, namely, a competition between an electronic density that drives the system toward more neutron rich nuclei and a nuclear symmetry energy that opposes such a change.

The toy model consists of the following two approximations. First, a simple liquid-drop model will be used to compute nuclear masses [see Eq. (2)]. Second, the electronic contribution will be assumed to be that of an extremely relativistic (i.e., $m_e/p_{\text{Fe}} \to 0$) Fermi gas. Although both of these approximations will be relaxed in the next section, we believe that the physical insights that one develops from this analytic treatment are valuable.

The liquid-drop mass formula may be written in the absence of pairing correlations [and by assuming $Z(Z-1) \approx Z^2$] as

follows:

$$\varepsilon_n(x, y) = m_p y + m_n(1-y) - a_v + \frac{a_s}{x} + a_c x^2 y^2 + a_a(1-2y)^2, \tag{19}$$

where $x \equiv A^{1/3}$ and $y \equiv Z/A$ is the proton (or electron) fraction. The various empirical constants (a_v, a_s, a_c, and a_a) represent volume, surface, Coulomb, and asymmetry contribution, respectively. Using a least-square fit to 2049 nuclei (available online at the UNEDF collaboration Web site `http://www.unedf.org/`) one obtains the following values for the four empirical constants:

$$\begin{aligned} a_v &= 15.71511\,\text{MeV}, \quad a_s = 17.53638\,\text{MeV}, \\ a_c &= 0.71363\,\text{MeV}, \quad a_a = 23.37837\,\text{MeV}. \end{aligned} \tag{20}$$

To understand the competition among the various terms—and to anticipate how this competition will be modified in the presence of a Fermi gas of electrons—we compute the optimal values of x and y using the simple liquid-drop formula by setting both derivatives equal to zero. That is,

$$\left(\frac{\partial \varepsilon_n}{\partial x}\right)_y = -\frac{a_s}{x^2} + 2a_c x y^2 = 0, \tag{21a}$$

$$\left(\frac{\partial \varepsilon_n}{\partial y}\right)_x = -\Delta m + 2a_c x^2 y - 4a_a(1-2y) = 0, \tag{21b}$$

where we have defined $\Delta m \equiv m_n - m_p$. This set of equations has the following simple analytic solution:

$$A = x^3 = \left(\frac{a_s}{2a_c}\right)\frac{1}{y^2}, \tag{22a}$$

$$y = \frac{1 + \left(\frac{\Delta m}{4a_a}\right)}{2 + \left(\frac{a_c}{2a_a}\right)x^2} \approx \frac{1/2}{1 + \left(\frac{a_c}{4a_a}\right)x^2}. \tag{22b}$$

These solutions suggest the following physical interpretation. For a fixed proton fraction $y = Z/A$, the optimal value of x emerges from a competition between the surface contribution (which favors large x) and the Coulomb contribution (which favors small x). For the set of empirical constants given in Eq. (20), the relevant ratio is given by $a_s/2a_c \approx 12.287$. Conversely, if $A = x^3$ is held fixed, then the optimal proton fraction y results from the competition between Coulomb and asymmetry contributions, with the former favoring $y = 0$ and the latter $y = 1/2$. If both equation are solved simultaneously, then one finds the most stable nucleus for this parameter set. One obtains $x_0 = 3.906$ and $y_0 = 0.454$, or, equivalently,

$$\begin{aligned} A_0 &= 59.598, \quad Z_0 = 27.060, \quad N_0 = 32.538, \\ (B/A)_0 &= 8.784\,\text{MeV}, \quad m_0 = 930.195\,\text{MeV}, \end{aligned} \tag{23}$$

with $m_0 \equiv (M/A)_0$ being the nuclear mass per nucleon.

The second assumption defining the toy model is that of an extremely relativistic Fermi gas of electrons (i.e., $p_{\text{Fe}} \gg m_e$). In this limit one obtains simple expressions for the total energy per baryon, chemical potential, and pressure in terms of the adopted set of variables. That is,

$$\varepsilon(x, y, p_F) = \varepsilon_n(x, y) + \frac{3}{4}y^{4/3}p_F - C_\ell\, x^2 y^2 p_F, \tag{24a}$$

$$\mu(x, y, p_F) = \varepsilon_n(x, y) + y^{4/3}p_F - \frac{4}{3}C_\ell\, x^2 y^2 p_F, \tag{24b}$$

$$P(x, y, p_F) = \frac{n}{4}y^{4/3}p_F - \frac{n}{3}C_\ell\, x^2 y^2 p_F. \tag{24c}$$

Before assessing the quantitative impact of the density-dependent (i.e., electronic and lattice) contributions on the semiempirical mass formula, a few comments are in order. First, at the predicted neutron drip density of about $4 \times 10^{11}\,\text{g/cm}^3$, the Fermi momentum is approximately equal to $p_F^{\max} \approx 40$ MeV. This suggests a large electronic contribution at those densities of about $\varepsilon_e^{\max} \approx 30\, y^{4/3}$ MeV. As the nuclear contribution is independent of density, the electrons will drive the system to small values of y. Second, the lattice contribution (perhaps not surprisingly) has the same dependence on x and y as the Coulomb contribution to the semiempirical mass formula. Indeed, the full impact of the lattice contribution can be included through a redefinition, albeit a density-dependent one, of the Coulomb coefficient. That is, $a_c \to \widetilde{a}_c(p_F) \equiv (a_c - C_\ell p_F)$. As the optimal value of the proton fraction y (for fixed x) emerges from a competition between Coulomb and asymmetry terms [see Eq. (22b)], the lattice contribution drives the system toward the symmetric $y = 1/2$ limit. Yet the lattice contribution is marginal. Indeed, even at neutron drip densities its contribution provides a meager, although by no means negligible, correction to the dominant Coulomb term. These two facts summarize the main structure of the outer crust, namely, a nuclear lattice embedded in an electron gas that is responsible for driving the system toward progressively more neutron rich nuclei. Thus the outer crust represents a unique laboratory for the study of neutron-rich nuclei in the $Z \approx 20$–50 region. As such, it nicely complements rare-isotope facilities worldwide that aim to provide a detailed map of the nuclear landscape.

Incorporating electronic and lattice contributions to the semiempirical mass formula yields the following expression for the total energy per nucleon of the system:

$$\varepsilon(x, y, p_F) = m_p y + m_n(1-y) - a_v + \frac{a_s}{x} + a_c x^2 y^2 + a_a(1-2y)^2 + \frac{3}{4}y^{4/3}p_F - C_\ell\, x^2 y^2 p_F. \tag{25}$$

As done before for the pure nuclear contribution, the optimal values of x and y—at fixed density—may be obtained by setting both derivatives equal to zero. That is,

$$\left(\frac{\partial \varepsilon}{\partial x}\right)_{y, p_F} = -\frac{a_s}{x^2} + 2\widetilde{a}_c x y^2 = 0, \tag{26a}$$

$$\left(\frac{\partial \varepsilon_n}{\partial y}\right)_{x, p_F} = -\Delta m + 2\widetilde{a}_c x^2 y - 4a_a(1-2y) + y^{1/3}p_F = 0, \tag{26b}$$

where a "renormalized" Coulomb coefficient has been defined as

$$\widetilde{a}_c(p_F) \equiv (a_c - C_\ell p_F). \tag{27}$$

1. First-order solution

Before providing exact solutions to Eqs. (26), we compute approximate solutions that are accurate to first order in p_F. In addition of being analytic, these closed-form expressions provide valuable insights into the composition of the outer crust. The first-order solutions are obtained by incorporating the density dependence in the following form:

$$x(p_F) = x_0(1+\xi) \quad \text{and} \quad y(p_F) = y_0(1+\eta), \tag{28}$$

where both ξ and η represent small (i.e., first-order in p_F) deviations from the zero-density results. Substituting these equations into Eqs. (26) yields the first-order solutions. One obtains

$$\begin{aligned} x(p_F) &= x_0\left[1+\left(\frac{(C_1-1)C_\ell+2C_2}{3C_1-1}\right)\frac{p_F}{a_c}\right] \\ &= (3.90610+0.03023\,p_F), \end{aligned} \tag{29a}$$

$$\begin{aligned} y(p_F) &= y_0\left[1-\left(\frac{3C_2-C_\ell}{3C_1-1}\right)\frac{p_F}{a_c}\right] \\ &= (0.45405-0.00419\,p_F). \end{aligned} \tag{29b}$$

Note that in these expressions the Fermi momentum should be given in MeV. Moreover, for simplicity the following two dimensionless quantities were introduced:

$$C_1 \equiv \frac{4a_a}{x_0^2 a_c} \approx 8.58843 \quad \text{and} \quad C_2 \equiv \frac{1}{2x_0^2 y_0^{2/3}} \approx 0.05547. \tag{30}$$

The first-order equations [Eqs. (29)]—while not necessarily quantitatively accurate—provide useful insights into how the composition of the outer crust evolves with density. As previously suggested, the proton fraction y decreases with density in an effort to minimize the "repulsive" electronic contribution. Indeed, to an excellent approximation Eq. (29b) may be written in the following simple form:

$$y(p_F) = y_0 - \frac{p_{\rm Fe}}{8a_a} = (0.45405 - 0.00411\,p_F). \tag{31}$$

As indicated in Eq. (22b), the optimal value of y_0 emerges from a competition between Coulomb and asymmetry terms, with the former driving y_0 toward zero and the latter toward one half. This equation indicates that the evolution of y with density is controlled by the dimensionless ratio of $p_{\rm Fe}/a_a$, suggesting that the larger the value of the asymmetry energy, the slower the evolution away from y_0, that is, the more symmetric the nucleus will remain. Moreover, as the denominator in Eq. (31) [$8a_a \approx 100$ MeV] is significantly larger than the electronic Fermi momentum over the entire region of interest, the first-order approximation is expected to be fairly accurate over the entire outer crust. Indeed, assuming a realistic value for the drip density of $\rho_{\rm drip} = 4\times10^{11}\,{\rm g/cm^3}$ yields a proton fraction of $y_{\rm drip} = 0.298$. This represents a 2% deviation from the value of $y(^{118}{\rm Kr}) = 0.305$ for the conventionally accepted drip nucleus ^{118}Kr.

2. Exact solution

The exact solution to the toy-model problem requires (for a fixed value of p_F) finding the simultaneous roots of Eqs. (26a) and (26b). Although the exact solution is numerically simple, it cannot be displayed in closed form. Yet the exact solution differs only slightly from the $C_\ell \equiv 0$ solution—which has an analytic, albeit a bit unorthodox, solution. The closed-form solution for the $C_\ell \equiv 0$ case may be obtained by simply rewriting Eqs. (26) as

$$x(y) = \left(\frac{a_s}{2a_c y^2}\right)^{1/3}, \tag{32a}$$

$$p_F(y) = \frac{\Delta m - 2a_c x^2 y + 4a_a(1-2y)}{y^{1/3}}. \tag{32b}$$

This set of equations suggests that rather than looking for a solution of x and y as a function of p_F, one should "solve" for x and p_F as a function of y, with the maximum value of y given by $y_{\rm max} = y_0 = 0.45405$ and the minimum value of y given by the condition $\mu(y_{\rm min}) = m_n$.

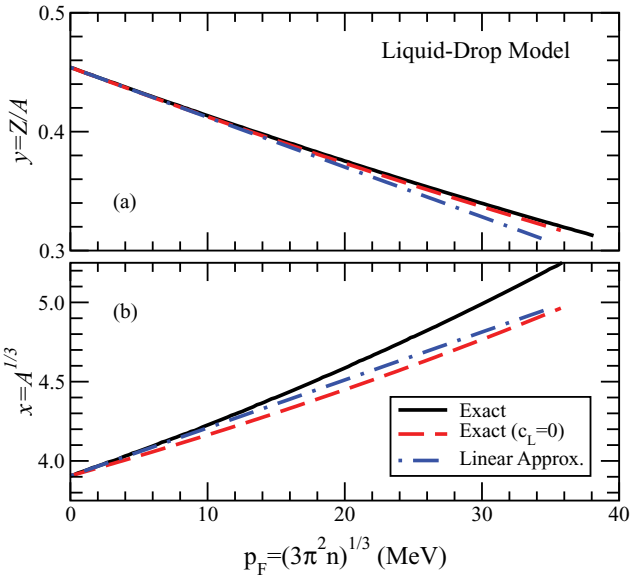

FIG. 2. (Color online) Proton fraction $y = Z/A$ (a) and baryon number $x = A^{1/3}$ (b) displayed as a function of the Fermi momentum $p_F \equiv (3\pi^2 n)^{1/3}$. The black solid lines represent the exact solution to the toy-model problem given in Eqs. (26), the red dashed lines display the corresponding solution in the $C_\ell \equiv 0$ (no lattice) limit [see Eqs. (32)], and the low-density solution [Eqs. (29)] is displayed by the blue dot-dashed lines.

In Fig. 2 the baryon number $x = A^{1/3}$ and proton fraction $y = Z/A$ are displayed as a function of the Fermi momentum $p_F \equiv (3\pi^2 n)^{1/3}$. The black solid line displays the exact numerical solution to the toy-model problem [see Eqs. (26)]. In this simple model, the drip line density is predicted to be at $\rho_{\rm drip} = 4\times10^{11}\,{\rm g/cm^3}$ with the drip line nucleus being ^{154}Cd (i.e., $Z = 48$ and $N = 106$). The solution obtained by ignoring the lattice contribution is displayed by the red dashed line. Because the lattice contribution to the chemical potential is negative, the $C_\ell \equiv 0$ solution reaches the drip line faster (i.e., at a lower density). Moreover, as the lattice contribution "renormalizes" the Coulomb term in the semiempirical mass formula (or, equivalently, enhances the role of the symmetry energy) the $C_\ell \equiv 0$ solution predicts a lower proton fraction

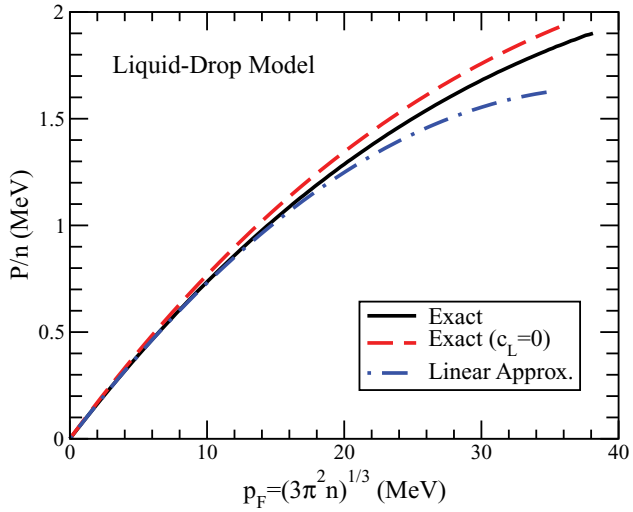

FIG. 3. (Color online) Pressure as a function of the Fermi momentum $p_F \equiv (3\pi^2 n)^{1/3}$. The black solid line represent the exact solution to the toy-model problem, the red dashed line displays the corresponding $C_\ell \equiv 0$ (no lattice) solution, and the low-density solution is displayed by the blue dot-dashed line.

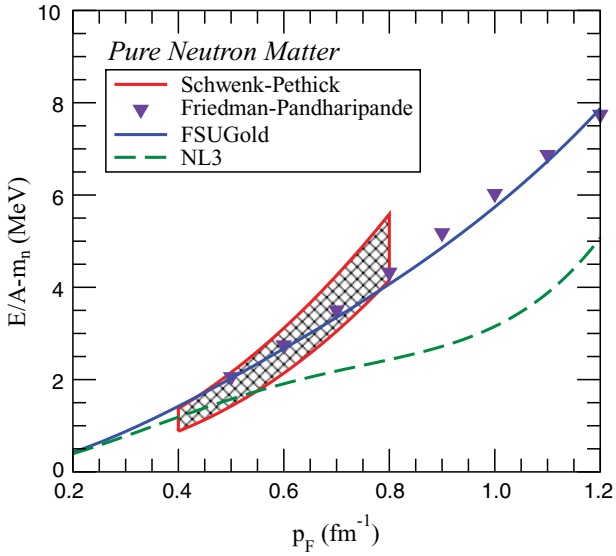

FIG. 4. (Color online) Energy per particle for pure neutron matter as a function of the neutron Fermi momentum. Shown are the microscopic model of Friedman and Pandharipande [46] (purple triangles) and the *model-independent* result based on the physics of resonant Fermi gases by Schwenk and Pethick [9] (red region). Also shown are the predictions from the accurately calibrated NL3 [13,14] (green dashed line) and FSUGold [15] (blue line) parameter sets.

than the exact solution. Finally, the dot-dashed blue line displays the solution correct to first order in p_F. In the particular case of the proton fraction y, the approximate linear solution $y = y_0 - p_{\rm Fe}/8a_a$ [Eq. (31)] reproduces fairly accurately the behavior of the exact solution.

The equation of state (i.e., pressure versus density) predicted by the toy model is displayed in Fig. 3. Because the lattice provides a negative contribution to the pressure [Eq. (24c)], the equation of state for the $C_\ell \equiv 0$ case is slightly stiffer than the exact one. The first-order solution in p_F provides a quantitatively accurate description of the equation of state up to fairly large values of the density. Note that the first-order approximation to the pressure is defined as follows:

$$\frac{P}{np_F} = \frac{1}{4}y^{4/3} - \frac{1}{3}C_\ell\, x^2 y^2 \approx (0.08367 - 0.00106 p_F). \quad (33)$$

B. Realistic models of the outer crust

In this section we employ realistic nuclear mass models to compute the structure and composition of the outer crust. Two of the models [41–45] are based on sophisticated mass formulas that have been calibrated to thousands of available experimental masses throughout the periodic table [39,40]. The other two models are based on accurately calibrated microscopic approaches that employ a handful of empirical parameters to reproduce the ground-state properties of finite nuclei and some nuclear collective excitations [13–15].

Whereas the microscopic models have yet to attain the level of precision displayed by the microscopic/macroscopic ones, they are valuable in elucidating various details of the underlying physics. For example, in the previous section we established the critical role played by the symmetry energy in the evolution of the proton fraction with density [see Eq. (31)]. However, it is unknown how the symmetry energy coefficient a_a changes as nuclei move toward the drip line. Presumably, the development of a significant neutron skin makes these nuclei (on average) more dilute than their stable counterparts. If so, one needs to extrapolate the symmetry energy to lower densities, a procedure that is highly uncertain because of our poor knowledge of the slope of the symmetry energy. To illustrate this uncertainty, the equations of state of pure neutron matter predicted by NL3 (green dashed line) and FSUGold (blue solid line) are displayed in Fig. 4. For comparison, we also show the predictions from the microscopic model of Friedman and Pandharipande based on realistic two-body interactions [46] (purple upside-down triangles) and the *model-independent* result based on the physics of resonant Fermi gases by Schwenk and Pethick [9] (red hatched region). Note that, to a very good approximation, the equation of state of pure neutron matter equals that of symmetric nuclear matter plus the symmetry energy. The differences between NL3 and FSUGold displayed in Fig. 4 are all due to the large uncertainties in the symmetry energy. In particular, as NL3 predicts a stiffer equation of state than FSUGold, namely, one whose energy increases faster with density at high densities, the symmetry energy of NL3 is lower than that of FSUGold at subsaturation densities. Thus, FSUGold has been shown to reach the neutron drip lines earlier than NL3 [47]. By the same token, NL3 should predict a sequence of more neutron rich nuclei (lower y) in the outer crust than FSUGold.

Shown in the left-hand panel of Fig. 5 is the proton fraction predicted by the two microscopic models, FSUGold (blue solid line) and NL3 (green dashed line). Also shown is the simple prediction obtained from the liquid-drop formula [Eq. (31)]. The proton fraction predicted with the FSUGold parameter

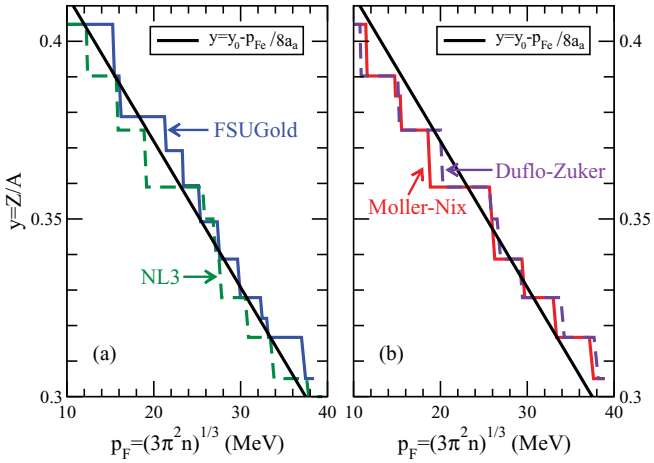

FIG. 5. (Color online) (a) The proton fraction predicted by the accurately calibrated FSUGold (blue solid line) and NL3 (green dashed line) parameter sets along with the simple liquid-drop formula given in Eq. (31). (b) The corresponding proton fraction as predicted by the mass formulas from Moller-Nix (red solid line) and Duflo-Zuker (purple dashed line).

set is consistently higher than for the NL3 set. This is a reflection of the stiffer penalty imposed on the FSUGold set for departing from the symmetric ($N = Z$) limit. The right-hand panel shows the corresponding behavior for the case of the microscopic/macroscopic models of Moller-Nix (red solid line) and Duflo-Zuker (purple dashed line). Differences among these two models are small.

Similar trends may be observed in Figs. 6 and 7, where the composition of the outer crust is displayed as a function of density. As the system makes a rapid jump in neutron number (say to magic number $N = 50$) the proton number

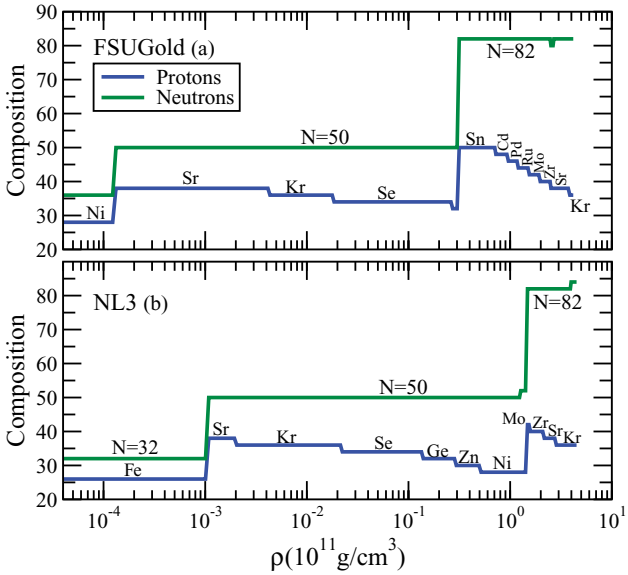

FIG. 6. (Color online) Composition of the outer crust of a neutron star as predicted by the accurately calibrated FSUGold (a) and NL3 (b) parameter sets. Protons are displayed with the (lower) blue line and neutrons with the (upper) green line.

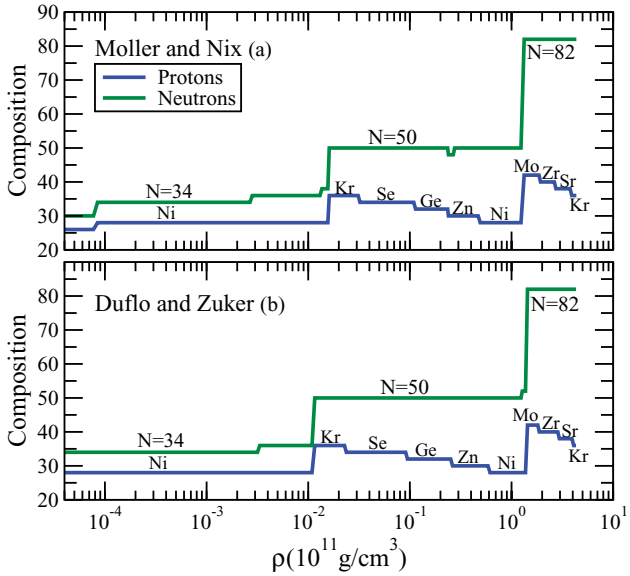

FIG. 7. (Color online) Composition of the outer crust of a neutron star as predicted by using the mass formulas of Moller-Nix (a) and Duflo-Zuker (b). Protons are displayed with the blue (lower) line and neutrons with the green (upper) line.

jumps with it. Along this neutron plateau, the proton fraction decreases systematically with increasing density in an effort to reduce the electronic contribution to the chemical potential. Eventually, the neutron-proton mismatch is too large and the jump to the next neutron plateau ensues—a jump that is driven by the symmetry energy. Clearly, the larger the symmetry energy is at low densities, the smaller is the neutron-proton mismatch and the earlier is the jump to the next neutron plateau. These features are clearly displayed in Fig. 6 as one contrasts the behavior of FSUGold to that of NL3. In contrast,

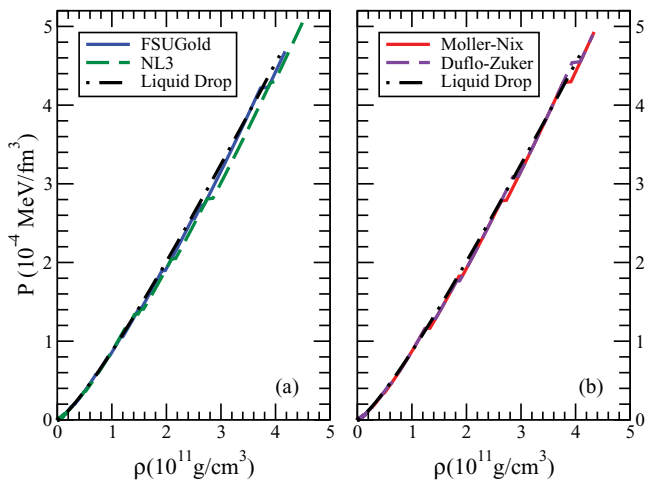

FIG. 8. (Color online) (a) The zero-temperature equation of state (pressure versus density) predicted by the accurately calibrated FSUGold (blue solid line) and NL3 (green dashed line) parameter sets along with the prediction from the simple liquid-drop formula. (b) The corresponding expression as predicted by the mass formulas from Moller-Nix (red solid line) and Duflo-Zuker (purple dashed line).

TABLE I. Equation-of-state observables (mass density, baryon density, pressure, and electronic chemical potential) and composition (nucleus and binding energy per nucleon) at the base of the outer crust.

Model	ρ (10^{11} g/cm^3)	n (10^{-4} fm^{-3})	P (10^{-4} MeV/fm^3)	μ_e (MeV)	Element	B/A (MeV)
Moller-Nix	4.34	2.60	4.93	26.22	^{118}Kr	7.21
Duflo-Zuker	4.32	2.58	4.89	26.17	^{118}Kr	7.19
FSUGold	4.17	2.50	4.68	25.88	^{118}Kr	7.11
NL3	4.49	2.69	5.06	26.39	^{120}Kr	7.13

few differences are noticeable in Fig. 7 when comparing the model of Moller-Nix to that of Duflo-Zuker.

We conclude this section by displaying in Fig. 8 equation-of-state (pressure-versus-density) predictions for the outer crust of a neutron star. The left-hand panel shows results from calculations using the FSUGold (blue solid line) and NL3 (green dashed line) parameter sets. Although barely visible, the density shows discontinuities at those places where the composition changes abruptly. It is also noted that the FSUGold parametrization predicts a pressure that rises slightly faster with density than that of NL3. For the NL3 set, the symmetry energy admits lower values of the proton/electron fraction y, which, in turn, lowers the pressure of the system. Lower values of y also yield lower values of the chemical potential, thereby delaying the arrival to the neutron drip line. Indeed, whereas FSUGold predicts a drip line density of $\rho_{\rm drip} = 4.17 \times 10^{11}$ g/cm^3, with NL3 the transition is delayed by about 8%, or until $\rho_{\rm drip} = 4.49 \times 10^{11}$ g/cm^3. A similar plot is shown for the microscopic/macroscopic models of Moller-Nix (red solid line) and Duflo-Zuker (purple dashed line). Differences between these two models are barely noticeable. Indeed, drip line densities in both models are predicted at about $\rho_{\rm drip} = 4.3 \times 10^{11}$ g/cm^3. Model predictions for various observables at the base of the outer crust (i.e., in the drip line region) are listed in Table I.

We remark in closing that all nuclei generated with the FSUGold parameter set included pairing correlations but neglected deformation. In regard to pairing correlations, these were included by means of a constant matrix element fitted to reproduce the experimental binding energies of some selected isotopic and isotonic chains, as described in Ref. [48]. However, deformation was ignored, so a spherical approximation was assumed in which all orbitals in the open shell share the same occupation number.

IV. CONCLUSIONS

Following the seminal work by Baym, Pethick, and Sutherland, as well as the more recent comprehensive work by Rüster, Hempel, and Schaffner-Bielich, we studied the composition and equation of state of the outer crust of nonaccreting neutron stars. The central focus of our study was the sensitivity of crustal properties to the density dependence of the symmetry energy. Four different models were adopted. Two of these models, Moller-Nix and Duflo-Zuker, are based on a combined microscopic/macroscopic approach and yield the most accurate nuclear masses available in the literature. The other two models, NL3 and FSUGold, are of a purely microscopic nature and are based on a relativistic mean-field approach. Although the former are significantly more accurate than the latter, microscopic models have the advantage of making definite predictions on how the symmetry energy changes with density (see Fig. 4). One can then study the impact of various features of the symmetry energy—such as its slope—on crustal properties.

The composition and equation of state of the outer crust emerge from a competition among three relatively simple contributions to the total energy (or chemical potential) of the system: nuclear, electronic, and lattice. The nuclear contribution appears exclusively in the form of nuclear masses and is independent of the baryon density. The electronic contribution is modeled after a zero-temperature free Fermi gas and dominates the behavior of the system with baryon density. Finally, the (body-centered-cubic) lattice contribution is also density dependent and provides a relatively modest correction (of no more than 10%) to the energy of the system. This competition is then primarily driven by an electronic term that favors a small electron fraction (to reduce the electronic Fermi energy) and a nuclear symmetry energy that opposes such a shift toward progressively more neutron rich nuclei. To motivate the discussion and to highlight this competition, we implemented a "toy model" of the outer crust by using a simple semiempirical ("Bethe-Weizsäcker") nuclear mass formula. Volume, surface, Coulomb, and asymmetry terms were extracted from a least-square fit to 2049 nuclei (see `http://www.unedf.org/`). The advantage of such a simple model is that useful insights emerge from the analytic structure of our results. Indeed, a particularly transparent result that illustrates nicely the competition between the electronic contribution and the nuclear symmetry energy was obtained, namely,

$$y(p_F) = y_0 - \frac{p_{\rm Fe}}{8a_a} + \mathcal{O}\left(p_{\rm Fe}^2\right), \tag{34}$$

where y_0 is the zero-density proton fraction, $p_{\rm Fe}$ is the electronic Fermi momentum, and a_a is the symmetry energy coefficient. Although illuminating, this (first-order) result is also surprisingly accurate, as the electronic Fermi momentum at the base of the outer crust is very close in value to the symmetry energy coefficient ($p_{\rm Fe} \approx 26$ MeV versus $a_a \approx 23$ MeV). In particular, the toy model predicts a value for the electron fraction at the base of the crust that differs by only a few percent from that of the drip line nucleus ^{118}Kr.

What is unknown, however, is how the symmetry energy coefficient a_a is modified as nuclei move away from the line of stability. Presumably, the symmetry energy is reduced in

neutron drip nuclei by the development of a dilute neutron skin. To investigate the sensitivity of the outer crust to the density dependence of the symmetry energy we employed two relativistic mean-field models (NL3 and FSUGold) that, although accurately calibrated, predict a significantly different density dependence for the symmetry energy. In particular, NL3 predicts a smaller symmetry energy than FSUGold at the (small) densities of relevance to the outer crust (see Fig. 4). One of the main goals of the present manuscript was to document how such differences impact the composition of the outer crust. One noticed, quite generally, that as the density increases along a fixed neutron-number plateau (say at magic number $N = 50$) the proton fraction decreased systematically in an effort to reduce the electronic contribution to the chemical potential. Eventually, however, the proton fraction becomes too low and the symmetry energy drives the system into the next plateau (say at magic number $N = 82$). How low can the proton fraction get is then a question that must be answered by the symmetry energy. Indeed, whereas NL3 predicts the formation of $^{78}_{28}\mathrm{Ni}_{50}$, FSUGold (having a larger symmetry energy) leaves the $N = 50$ plateau with the formation of $^{82}_{32}\mathrm{Ge}_{50}$ (or four protons earlier). This result may be stated in the form of a correlation between the neutron radius of ^{208}Pb and the composition of the outer crust: *The larger the neutron skin of* ^{208}Pb, *the more exotic the composition of the outer crust*. Note that by "exotic" we mean nuclei that are unstable under normal laboratory conditions. Finally, and as was done in Ref. [31], we have computed crustal properties using two of the most accurate tables of nuclear masses available today, namely, those of Moller-Nix and Duflo-Zuker. Our results using the model of Moller and Nix agree well with those published in Ref. [31]. These results are practically indistinguishable from the ones obtained using the Duflo-Zuker nuclear mass table, a table that includes 9210 nuclei!

In summary, we have used realistic nuclear mass tables to elucidate the role of the symmetry energy on the structure and composition of the outer crust of neutron stars. Recent observations of crustal modes in magnetars are likely to provide stringent limits on the equation of state of neutron-rich matter. As the field of nuclear astrophysics continues to advance—with the commission of both radioactive beam facilities as well as ground- and space-based telescopes—we enter a new era that promises great hope in the determination of the nuclear matter equation of state.

ACKNOWLEDGMENTS

The authors are grateful to José Barea, Alejandro Frank, Jorge Hirsch, and their students for useful discussions and for making the Duflo-Zuker mass formula available to us. We are also grateful to George Lalazissis for providing the NL3 mass formula. Xavier Roca-Maza acknowledges support from Grant Nos. AP2005-4751 and FIS2005-03142 from MEC (Spain) and FEDER. This work was supported in part by the Department of Energy Grant No. DE-FD05-92ER40750.

[1] J. M. Lattimer and M. Prakash, Astrophys. J. **550**, 426 (2001).
[2] J. M. Lattimer and M. Prakash, Science **304**, 536 (2004).
[3] G. Baym, C. Pethick, and P. Sutherland, Astrophys. J. **170**, 299 (1971).
[4] D. G. Ravenhall, C. J. Pethick, and J. R. Wilson, Phys. Rev. Lett. **50**, 2066 (1983).
[5] M. Hashimoto, H. Seki, and M. Yamada, Prog. Theor. Phys. **71**, 320 (1984).
[6] C. P. Lorenz, D. G. Ravenhall, and C. J. Pethick, Phys. Rev. Lett. **70**, 379 (1993).
[7] M. G. Alford, K. Rajagopal, and F. Wilczek, Nucl. Phys. **B537**, 443 (1999).
[8] K. Rajagopal and F. Wilczek, The Condensed Matter Physics of QCD, At the Frontier of Particle Physics, Handbook of QCD, edited by M. Shifman (World Scientific, 2000), Vol. 4, hep-ph/0011333.
[9] A. Schwenk and C. J. Pethick, Phys. Rev. Lett. **95**, 160401 (2005).
[10] J. Piekarewicz, Phys. Rev. C **76**, 064310 (2007).
[11] B. A. Brown, Phys. Rev. Lett. **85**, 5296 (2000).
[12] R. J. Furnstahl, Nucl. Phys. **A706**, 85 (2002).
[13] G. A. Lalazissis, J. Konig, and P. Ring, Phys. Rev. C **55**, 540 (1997).
[14] G. A. Lalazissis, S. Raman, and P. Ring, At. Data Nucl. Data Tables **71**, 1 (1999).
[15] B. G. Todd-Rutel and J. Piekarewicz, Phys. Rev. Lett. **95**, 122501 (2005).
[16] C. J. Horowitz, S. J. Pollock, P. A. Souder, and R. Michaels, Phys. Rev. C **63**, 025501 (2001).
[17] Jefferson Laboratory experiment E-00-003, spokespersons R. Michaels, P. A. Souder, and G. M. Urciuoli (2005); http://hallaweb.jlab.org/parity/prex.
[18] C. J. Horowitz and J. Piekarewicz, Phys. Rev. Lett. **86**, 5647 (2001).
[19] C. J. Horowitz and J. Piekarewicz, Phys. Rev. C **64**, 062802(R) (2001).
[20] C. J. Horowitz and J. Piekarewicz, Phys. Rev. C **66**, 055803 (2002).
[21] J. Carriere, C. J. Horowitz, and J. Piekarewicz, Astrophys. J. **593**, 463 (2003).
[22] A. W. Steiner, M. Prakash, J. M. Lattimer, and P. J. Ellis, Phys. Rep. **411**, 325 (2005).
[23] A. W. Steiner, Phys. Rev. C **77**, 035805 (2008).
[24] A. L. Piro, Astrophys. J. **634**, L153 (2005).
[25] T. E. Strohmayer and A. L. Watts, Astrophys. J. **653**, 593 (2006).
[26] A. L. Watts and T. E. Strohmayer, Astrophys. Space Sci. **308**, 625 (2007).
[27] A. L. Watts and T. E. Strohmayer, Adv. Space Res. **40**, 1446 (2007).
[28] C. Thompson and R. C. Duncan, Mon. Not. R. Astron. Soc. **275**, 255 (1995).
[29] C. Kouveliotou *et al*., Nature (London) **393**, 235 (1998).
[30] C. Kouveliotou, R. C. Duncan, and C. Thompson, Sci. Am. **288N2**, 24 (2003).
[31] S. B. Rüster, M. Hempel, and J. Schaffner-Bielich, Phys. Rev. C **73**, 035804 (2006).
[32] P. Haensel, J. L. Zdunik, and J. Dobaczewski, Astron. Astrophys. **222**, 353 (1989).

[33] P. Haensel and B. Pichon, Astron. Astrophys. **283**, 313 (1994).
[34] E. Wigner, Phys. Rev. **46**, 1002 (1934).
[35] E. Wigner, Trans. Faraday Soc. **34**, 678 (1938).
[36] A. L. Fetter and J. D. Walecka, *Quantum Theory of Many Particle Systems* (McGraw-Hill, New York, 1971).
[37] R. A. Coldwell-Horsfall and A. A. Maradudin, J. Math. Phys. **1**, 395 (1960).
[38] C. A. Sholl, Proc. Phys. Soc. **92**, 434 (1967).
[39] G. Audi and A. H. Wapstra, Nucl. Phys. **A565**, 1 (1993).
[40] G. Audi and A. H. Wapstra, Nucl. Phys. **A595**, 409 (1995).
[41] J. Duflo, Nucl. Phys. **A576**, 29 (1994).
[42] A. Zuker, Nucl. Phys. **A576**, 65 (1994).
[43] J. Duflo and A. P. Zuker, Phys. Rev. C **52**, R23 (1995).
[44] P. Moller, J. R. Nix, W. D. Myers, and W. J. Swiatecki, At. Data Nucl. Data Tables **59**, 185 (1995).
[45] P. Moller, J. R. Nix, and K. L. Kratz, At. Data Nucl. Data Tables **66**, 131 (1996).
[46] B. Friedman and V. R. Pandharipande, Nucl. Phys. **A361**, 502 (1981).
[47] B. G. Todd and J. Piekarewicz, Phys. Rev. C **67**, 044317 (2003).
[48] M. Del Estal, M. Centelles, X. Viñas, and S. K. Patra, Phys. Rev. C **63**, 044321 (2001).